Production of lignocellulose nanofibrils by conventional and microwave-assisted deep-eutectic-solvent pretreatments: mechanical, antioxidant, and UV-blocking properties

Gu-Joong Kwon
Kangwon Institute of Inclusion Technology, Kangwon National University
Seung-Woo Cho
Kangwon National University
Rajkumar Bandi
Kangwon National University
Bong-Suk Yang
Dongguk University
Ramakrishna Dadigala
Kangwon National University
Song-Yi Han
Kangwon National University
Seo-Young Ma
Kangwon National University
Jeong-Ki Kim
Kangwon National University
Nam-Hun Kim
Kangwon National University
Seung-Hwan Lee (lshyhk@kangwon.ac.kr)
Kangwon Institute of Inclusion Technology, Kangwon National University

Research Article

Keywords: lignocellulose nanofibrils, microwave heating, deep eutectic solvents, food packaging

Posted Date: December 6th, 2022

DOI: https://doi.org/10.21203/rs.3.rs-2336277/v1

Additional Declarations: No competing interests reported.

Version of Record: A version of this preprint was published at Cellulose on April 1st, 2023. See the published version at https://doi.org/10.1007/s10570-023-05164-1.

Abstract

Herein for the first time, lignocellulose nanofibrils (LCNF) were prepared from pine-wood powder using microwave (MW)-assisted deep eutectic solvent (DES) pretreatment coupled with high-pressure homogenization. A DES based on choline chloride and lactic acid was employed, and LCNFs prepared by conventional DES pretreatment at 110°C (LCNF-110) and 130°C (LCNF-130) were used for comparison. Although MW treatment offered a high removal of lignin (70%) and hemicellulose (90%) within a short time (110 s), the morphological observations by scanning and transmission electron microscopies revealed excellent defibrillation of the conventionally heat-treated samples. Likewise, LCNF-110 and LCNF-130 exhibited high tensile strengths of 154.6 ± 5.0 and 136.8 ± 1.2 MPa, respectively, whereas that of LCNF-MW was only 75.6 ± 1.4 MPa. Interestingly, LCNF-MW with a lignin content between that of LCNF-110 and LCNF-130 exhibited high thermal stability (T_{max} 309.6°C) and potent antioxidant properties. However, the lignin contents of the LCNFs determined their UV-radiation blocking efficiency, where LCNF-110 > LCNF-MW > LCNF-130. Furthermore, all LCNF films exhibited good visible-light transparency, flexibility, and water contact angles (> 87°), indicating their promising potential for packaging applications.

Introduction

The production and application of lignin-containing cellulose nanofibrils (LCNFs) has become the latest trend in nanocellulose research. This popularity can be credited to their low environmental impact, high production yield, and more novel applications compared to those of pure cellulose nanofibrils (Rojo et al. 2015; Trovagunta et al. 2020). LCNFs can be directly isolated from unbleached lignocellulosic biomass, thus avoiding complicated delignification processes. Lignin retention is known to improve the thermal, mechanical and barrier properties (Nair and Yan 2015a; Wang et al. 2018). Furthermore, lignin endows the cellulose nanofibrils with UV protection, hydrophobicity, and antioxidant and antimicrobial properties (Gu et al. 2019; Sirviö et al. 2020; Bian et al. 2021). Nair et al. isolated LCNFs with a high modulus and good barrier properties from bark using alkali and chlorite treatment coupled with mechanical fibrillation (Nair and Yan 2015b). Herrera et al. isolated LCNFs with a high lignin content of 23% from eucalyptus pulp through 4-acetamido-TEMPO-mediated oxidation coupled with high-pressure homogenization (Herrera et al. 2018). These LCNFs were found to be suitable for the preparation of nanopapers with low oxygen permeability. Wen et al. used a sequential process of TEMPO-oxidation and high-pressure homogenization to isolate LCNFs from poplar pulp (Wen et al. 2019). The LCNFs exhibited high hydrophobicity and thermal stability and were less gel-like than CNFs. However, these strategies involve the usage of corrosive chemicals in large quantities, posing an environmental burden. Hence it is essential to explore more eco-friendly strategies for LCNF production.

Recently, deep eutectic solvent (DES) pretreatment has emerged as a promising method for LCNF production. A DES is a blend of two or more components with a low eutectic point (Francisco et al. 2012; Lynam et al. 2017). They can be simply prepared by mixing a hydrogen bond acceptor (HBA) and hydrogen bond donor (HBD) (Abbott et al. 2003; Smith et al. 2014). DESs offer various advantages such

as facile preparation at low cost, low vapor pressure, non-flammability, and recyclability (Liu et al. 2017b; Wang et al. 2020). DESs can efficiently dissolve the constituents of lignocellulose, especially lignin, and are capable of forming strong hydrogen bonds. This leads to a disruption of the hydrogen-bonding network, resulting in the dissolution of cellulose, hemicellulose, and lignin in the DES (Sirviö et al. 2015; Alvarez-Vasco et al. 2016; Kumar et al. 2016; Chen et al. 2018). DESs are more suitable for the dissolution of lignin and hemicellulose, leaving the cellulose-rich portion undissolved, which can be used for LCNF preparation. An extensive molecular library of HBDs and HBAs for DES production has been compiled (Zdanowicz et al. 2018; Satlewal et al. 2018). Among them, DESs based on choline chloride (ChCl) and lactic acid (LA) have been extensively studied, and the literature suggests that ChCl-LA-based DES pretreatment is an efficient method to extract lignin from biomass (Kwon et al. 2020, 2021; Liu et al. 2020).

Compared with conventional heating, microwave irradiation allows rapid and uniform heat transfer through dipole rotation and ionic conduction with low energy conduction (Liu et al. 2019b). Microwave irradiation has been shown to greatly enhance the ionic properties and molecular polarity of DESs, thereby reducing the reaction time and temperature (Aguilar-Reynosa et al. 2017). Hence, combining DESs with microwave heating in lignocellulose pretreatment offers the potential for efficient and sustainable LCNF production. Liu et al. reported the preparation of LCNFs from energy cane bagasse (ECB) using microwave-assisted DES treatment coupled with ultrasonication (Liu et al. 2020). A ChCl/LA (1:10) DES heated at 110°C for 30 min was found to be the optimal pretreatment (45.2% yield and 81.0% delignification) for LCNF production. LCNFs were applied to reinforce polyanionic cellulose film, improving its mechanical and UV-absorption properties. The authors also prepared LCNF from ECB using microwave-assisted natural DES pretreatment coupled with microfluidization (Liu et al. 2022a). In a recent report, the same research team prepared LCNFs and LCNCs using MW-DES pretreatment coupled with high-pressure homogenization of ECB and bleached wood pulp, respectively (Liu et al. 2022b). Ji et al. reported the efficient cleavage of strong hydrogen bonds in sugarcane bagasse by MW-assisted ternary acidic DES pretreatment and subsequent ultrasonication to produce LCNF (Ji et al. 2021). LCNFs with high thermal stability were obtain upon treatment at 100°C for 20 min.

Inspired by these studies, we attempted an MW-assisted DES pretreatment of a pine wood sample and subsequent defibrillation to prepare LCNFs. To the best of our knowledge, this is the first report on this specific approach. All the previously reported methods explored the use of bleached pulp or bagasse, which were either already exposed to some pretreatment or weak. Furthermore, all these methods used a MW reactor, which requires high capital cost, and no comparison with conventional heating has been made, so the true advantage of MW is unknown. In the present work, a custom-made Teflon vessel was used along with a domestic microwave oven; its performance was compared with that of conventional heating. The basic characteristics of the LCNFs, including their morphological, chemical, and thermal properties, were studied first. Furthermore, the lignin-specific and application-oriented properties, such as hydrophobicity, UV-blocking ability, and antioxidant activity, were also explored.

Experimental Section

Materials

Red pine (*Pinus densiflora*) was collected from the Research Forest of Kangwon National University, Korea. An 8 cm thick disk was ground to a 40–80 mesh size, sealed in a plastic container, and stored in a dry place. Before DES pretreatment, extractives in the wood powder were removed by alcohol/benzene (1:2) extraction. ChCl (> 99%) and LA (extra pure grade, 90%) were acquired from Daejung Chemical (Siheung, Korea). All chemicals were used as received without any additional purification.

DES pretreatment

ChCl and LA acted as the HBA and HBD, respectively. They were mixed in molar ratios of 1:1, 1:3, and 1:5 and treated at 90 ℃ for 10 min under continuous stirring at 300 rpm until perfectly transparent liquids were formed. In the conventional heating method, 1 g of wood powder was added to 20 mL of DES in a 500 mL round bottomed flask, which was then placed in a heating mantle. The mixture was heated for 2 h at 110 ℃ and 2 h at 130 ℃ under continuous stirring at 300 rpm. In the MW method, 1 g of wood powder was added to 20 mL of DES in a 100 mL Teflon sample holder and treated for 80–110 s in a household MW (LG, MW23GD) at an output of 400 W. The maximum power output of the MW was 1.0 kW, and the operating frequency was 2450 MHz. To ensure thorough mixing of the contents, the sample and DES were mixed and left to stand for one hour before MW treatment. The mixture was irradiated using a 10 s pulse time and 10 s interval. The treatment was not performed beyond 110 s, and a high output wattage was not applied because the Teflon container began to leak and eventually exploded as a result of pressure buildup under these conditions. Leakage was also observed in a previous study that also involved a MW pressure cooker (Impoolsup et al. 2020). If a leakage is detected, treatment should be immediately terminated. The DES pretreated samples were centrifuged (Supra 22 K; Hanil Scientific Inc., Gimpo, Korea) at 8000 rpm for 10 min to separate the lignin-rich soluble fraction. The cellulose-rich insoluble fraction was washed three times with 1,4-dioxane/water (4:1) and five times with deionized water (DW), and then freeze-dried for LCNF production. The yield of the solid residue was calculated using the following equation:

% Yield = (mass after DES pretreatment/initial mass of raw material) × 100%

LCNF preparation by mechanical defibrillation

A high-speed blender and high-pressure homogenizer were employed to produce LCNFs by mechanical defibrillation. The samples were diluted to 1.0 wt% by DW and blended at a rotation speed of 35,000 rpm for 30 min in a high-speed blender (HR-3752; Koninklijke Philips N.V., Amsterdam, Netherlands). Then, the suspension was further diluted to 0.1 wt% and defibrillated at an operating pressure of 20,000 psi using a high-pressure homogenizer (MN400BF; PICOMAX, Seoul, Korea) with a nozzle size of 100 μm. Five passes of the homogenization process were carried out.

Film preparation

The films were prepared using a vacuum filtration system comprising a vacuum pump and glass microanalysis filter holders (KGS-47; Advantec MFS Inc., Dublin, CA, USA). The LCNF suspensions were diluted to a solid content of 0.1 wt% (137.5 mL), sonicated for 1 min, and filtered through a silicone-coated filter (Whatman No. 2200 125; GE Healthcare Ltd., Buckinghamshire, UK). Vacuum was then applied (700 mmHg = 96 kPa) until free water was completely removed. The filtered LCNFs were placed between silicon-coated filters and hot-pressed for 1 min at 105°C and 15 MPa (Hankuk S and I Co. Ltd., Hwaseong, Korea) to obtain a film with a diameter of 35 mm.

Cellulose and hemicellulose content analysis using high-performance liquid chromatography

Sugar analysis was performed using Bio-LC (ICS-3000; Dionex, Sunnyvale, CA, USA) according to the National Renewable Energy Laboratory protocol (A. Sluiter, B. Hames, R. Ruiz et al. 2008). High-performance anion-exchange chromatography coupled with electrochemical detection based on pulsed amperometry (gold electrode) was used to quantify the neutral sugar. The sample was chromatographed on a CarboPac PA-1 column (Dionex). The system was operated in isocratic mode at a flow rate of 1.0 mL/min using a mixture of 250 mM sodium hydroxide (20%) and DW (80%). The contents of five types of sugars (glucose, xylose, arabinose, galactose, and mannose) were calculated using the Chromeleon software program (Version 6.8; Dionex). Glucose content was used for cellulose determination, and the sum of the contents of the other sugars (xylose, arabinose, galactose, and mannose) was used for hemicellulose determination.

Klason lignin quantitation using the TAPPI standard method

Lignin content was determined using a scaled-down version of the Klason protocol for the TAPPI standard method T222om-88 (2011). Briefly, 0.2 g of sample was treated with 3 mL of 72% H_2SO_4 for 2 h at room temperature (23–25°C). The solution was then diluted with 112 mL of DW and autoclaved at 121 ℃ for 1 h. The solid was filtered through a 1G4 glass filter and dried overnight at 105 ℃. The acid-insoluble lignin content was determined by the ratio between the weights of the solid residue and the initial amount of sample. The acid-soluble lignin was characterized using a UV–vis spectrophotometer (Lamda 35; PerkinElmer, Inc., Waltham, MA, USA) at an excitation wavelength of 205 mm.

X-ray diffraction (XRD) analysis

XRD analysis was performed using an X-ray diffractometer (DMAX 2100 V; Rigaku, Tokyo, Japan) operating with Cu Kα radiation (40 kV, 30 mA). Scans were taken over a 2θ (Bragg angle) range of 10–35° at a scanning speed of 1°/min. The crystallinity index (CrI) was calculated from the peak intensity of the crystalline-plane (200) diffraction (I_{200}) at 22.5° and from the minimum intensity at ≈ 18.0°, which is associated with the amorphous fraction of CNF (I_{am}) according to Segal et al. (1959).

$$CrI\ (\%) = I_{200} - I_{am} / I_{200}) \times 100$$

I_{200}: Diffraction intensity of (200) ($2\theta = 22.5°$)

I_{am}: Diffraction intensity of amorphous region (at the minimum intensity near $2\theta = 18°$)

The crystallite widths were estimated using the Scherrer equation with a constant (K) equal to 0.9 at the half-width peak of the (200) plane at $2\theta = 22.5°$, as follows:

$L = K\lambda/\beta\cos\theta$

where L is the crystallite width, θ is the Bragg angle peak position (2θ max position) in radians, λ is the wavelength of the radiation (0.1542 nm), K is a constant (0.9), and β is the peak width of the (200) profile at half-maximum (FWHM) in radians.

Electron microscopy

The LCNF suspension was diluted to 0.001 wt% and sonicated using an ultrasonicator (VCX130PB, Sonics & Materials Inc., USA) for 1 min. The suspension was vacuum-filtrated on a PTFE membrane filter, which was then immersed in *tert*-butyl alcohol for 30 min. The *tert*-butyl alcohol was replaced three times to completely exchange the water. The LCNFs were dried at − 55 ℃ for 3 h using a freeze dryer (FDB-5502, Operon Co. LTD., Gimpo, Republic of Korea). The dried LCNFs were fixed on metal stubs using carbon tape and coated with iridium alloy using a sputter coater (LEICA EM ACE600, Leica Microsystems, Germany). SEM images were acquired using a field-emission scanning electron microscope (FESEM; Hitachi S-4800, Japan) with an accelerating voltage of 5 kV and working distance of 5 mm.

Specimens for transmission electron microscopy (TEM) were diluted and sonicated to disperse the particles. TEM grids (200 mesh carbon film, copper) were floated on drops of ≈ 4 μL of sample for 1–2 min. The samples were then rinsed with DW and negatively stained with 2% uranyl acetate for 3 min. The samples were imaged using a field-emission transmission electron microscope (FETEM; JEM-2100F; Jeol, Tokyo, Japan) with an accelerating voltage of 200 kV. The width of the LCNF was measured using the Image J program (version 1.52).

Fourier-transform infrared (FT-IR) spectroscopic analysis

FTIR spectra of the DES-pretreated samples and LCNF films were recorded on a FT-IR instrument (Frontier 10; PerkinElmer, Inc.) in the range of 600–4000 cm^{-1} with a resolution of 4 cm^{-1}. The attenuated total reflection (ATR) method was used for the measurement. A total of 32 scans were collected for each sample.

Thermogravimetric analysis

Thermogravimetric analysis (TGA) of the LCNF sheets was performed using a thermogravimetric analyzer (SDT Q600; TA Instruments, New Castle, DE, USA). The temperature was controlled from 30 to 600 ℃ at a heating rate of 10 ℃/min. A high-purity nitrogen stream with a rate of 100 mL/min was continuously passed into the furnace to prevent any unwanted oxidation.

Tensile test

For the tensile test, a test piece with a size between 5.0–9.0 mm and 0.7–0.8 mm (width × thickness) was cut from at least five nanosheets and stored under constant temperature and humidity (25°C and 50% relative humidity). The tensile strength was measured for approximately one week after preparation. The tensile test was performed using a strength tester (H50K; Hounsfield Test Equipment, Redhill, UK) at a crosshead speed of 5 mm/min with a test-piece span of 50 mm.

UV – Vis spectroscopy

The UV – vis transmittance spectra of the LCNF films were measured using a Jasco V-550 spectrophotometer in the wavelength range of 190 – 900 nm.

Contact angle

The static water-contact angles of the LCNF films were measured using a contact-angle meter (Theta Lite, Biolin Scientific), and the volume of each droplet was 2 µL. Each contact angle was measured at 60 s; the average value of at least three measurements is presented.

Antioxidant activity

The antioxidant activities of the samples were assessed by their ability to inhibit the 2,2′-azino-bis (3-ethylbenzthiazoline-6-sulfonic acid) (ABTS) radical cation (Farooq et al. 2019). Firstly, ABTS was dissolved in water to a concentration of 7 mM. Then, the ABTS radical cation ($ABTS^{\bullet+}$) was produced by reacting ABTS stock solution with 2.45 mM potassium persulfate (1:0.5) and allowing the mixture to stand in the dark at room temperature for 16 h. The solution of the radical cation was then diluted with water until an initial absorbance of 0.7 ± 0.02 at 734 nm was reached. For analysis, the sample was added to 2 mL of the diluted radical solution, and this mixture was kept in the dark for 30 min. Then, the sample was removed from the suspension, and the absorbance at 734 nm was measured after 6 min.

The inhibition percentage of $ABTS^{\bullet+}$ was calculated using the following formula:

$$\text{Inhibition (\%)} = \frac{A_0 - A_1}{A_0} \times 100$$

where A_0 and A_1 are the absorbance of $ABTS^{\bullet+}$ before and after incubation, respectively, with the CNF films.

Results And Discussion

Yield of the solid residue

Figure 1 shows the yield of the solid residue obtained after DES pretreatment at different conditions under MW and conventional heating. The MW power and irradiation time were limited to 400 W and 110

s, respectively. As previously mentioned, the reaction was uncontrollable at higher wattages and longer reaction times, leading to destruction of the Teflon container. Furthermore, the reaction was controlled by irradiating for 10 s followed by a 10 s rest period. At 110°C, with an increase in mole ratio from 1:1 to 1:3, the yield decreased from 65.5–59.1%. A further increase in the ratio to 1:5 resulted in a 56.9% yield. Similarly, at 130°C, changing the mole ratio from 1:1 to 1:3 and 1:5 produced yields of 53.1, 42.3, and 40.2%, respectively. With an increase in lactic acid content, the yield decreased, which can be ascribed to the increase in acidity (Hong et al. 2020a). This change is more pronounced upon increasing the mole ratio from 1:1 to 1:3 than from 1:3 to 1:5. At each mole ratio, the yields at 110°C were less than those at 130°C, indicating that temperature has an effect; this is expected because high-temperature treatment is known to dissolve more lignin and sugars from wood powder. Furthermore, the temperature effect is more significant than the effect of the mole ratio, and this observation is in good agreement with previous reports (Kwon et al. 2021). Similarly, in the case of MW irradiation, at irradiation times of 80, 90, and 100 s, the yields remained 80.4, 78.1, and 69.8% respectively. However, a further increase in the irradiation time to 110 s drastically decreased the yield to 42.9%. This sudden decrease can be ascribed to two factors: (i) MW irradiation produces rapid and localized super heating, which might result in a sudden increase in the temperature, and (ii) lignin dissolution is highest at a temperature near the glass-transition temperature. In a previous study, Liu et al. noted a drastic decrease in the yield (from 56.1–36.5%) when the temperature was increased from 90°C to 130°C (Liu et al. 2020). The effect of CC/LA mole ratio was studied at 110 s MW irradiation. Upon increasing mole ratio from 1:1 to 1:3 and 1:5, the yield decreased from 62.1–50.8% and 42.9%. Unlike conventional heating, lactic acid content has a remarkable influence on yield under MW irradiation.

Chemical composition

Figure 2 shows the cellulose, hemicellulose, and lignin contents of pine wood before and after DES pretreatment by MW heating and conventional heating. The change in the main chemical composition of pine wood as a result of DES treatment is noticeable. The linear polysaccharide cellulose, heterogeneous hemicellulose, and structurally variable lignin are key components of the wood cell wall, which is interconnected by hydrogen bonding networks (between cellulose and hemicellulose) and covalent bonds (lignin and hemicellulose). Using conventional heating, an increase in temperature and LA content decreased the cellulose, hemicellulose, and lignin contents. It can be seen that temperature has a much greater influence than mole ratio. This finding is in accordance with those previous studies (Kwon et al. 2021). Using MW, the reduction of cellulose, hemicellulose, and lignin contents was negligible until 100 s and were greatly reduced at 110 s, which matches the trend in solid residue yield. Interestingly, the lignin and hemicellulose contents drastically decreased compared with the cellulose content. This might be due to localized superheating, causing the cleavage of the lignin–hemicellulose complex (Liu et al. 2017a), which was reported in other studies. The highest and lowest extents of lignin/cellulose removal were achieved by conventionally heating at 130 and 110°C, respectively; MW heating produced intermediate results. In the case of hemicellulose, 90.5% was removed under MW heating, while 89.6% and 72.7% was removed at 130 and 110°C, respectively.

The changes in the surface microscopic features of wood powder after DES pretreatment were studied using SEM. As shown in Fig. S1, before DES treatment, the surface appeared smooth and firm; by contrast, the surface appeared rough and the microfibers became exposed after DES treatment. This can be ascribed to the removal of hemicellulose and lignin. In both conventional and MW heating, the surface roughness and fiber exposure increased with LA content. High destruction and fiber exposure occurred at 130°C using a ChCl/LA mole ratio of 1:5, which is in good agreement with the low yield and high lignin and hemicellulose removal efficiencies under this condition. The DES-treated residues obtained using a ChCl/LA mole ratio of 1:5 were selected for LCNF production. The LCNFs obtained from the MW-treated sample is designated as LCNF-MW, and those produced from the conventionally heated sample are designated as LCNF-110 and LCNF-130 according to the pretreatment temperature.

Morphological characteristics

The morphological features of the LCNFs produced using the MW-treated and conventionally heat-treated samples were first explored using SEM and TEM analysis. As shown in Fig. 3, the SEM images reveal that all the samples contain nanofibrils with an entangled web-like structure. However, LCNF-MW exhibited some microfibers along with nanofibrils, indicating the inefficient defibrillation of the MW-treated sample. The TEM images and corresponding diameter-distribution histograms are presented in Fig. 3. The LCNFs appear as well-dispersed nanofibrils with an entangled network-like structure, and lignin nanoparticles were attached to their surface. The individual nanofibrils were a few microns in length and had diameters in the range of 6–60 nm. LCNF-MW exhibited a broad size distribution, and fibers with diameters of 60–90 nm were also observed. These results confirm the inefficient defibrillation of the microwave-treated sample. In general, residual lignin is known to act as a binder and protect cellulose from mechanical defibrillation, and higher lignin content is associated with inefficient defibrillation (Herrera et al. 2018). However, in the present study, despite its low lignin content compared to the 110°C treated sample, the MW-treated sample exhibited inefficient defibrillation. This observation suggests that lignin content alone is insufficient to judge the defibrillation efficiency of the DES-treated sample. Apart from lignin removal, DES can also swell the cellulose portion by forming hydrogen bonds. In detail, DES pretreatment can break the hydrogen-bond links between cellulose, which results in the softening and separation of fibrils and makes it more susceptible to defibrillation (Xie et al. 2023). We assume that this swelling effect was not prominent in the MW pretreatment owing to its short contact time and resultant inefficient defibrillation.

XRD analysis

The effect MW and conventional heat on the crystallinity and crystal structure of the DES was studied using XRD. XRD patterns of the raw material and LCNFs are presented in Fig. 4, and the corresponding crystallinity index and crystal widths are provided in Table 1. As shown in the figure, all the samples exhibited characteristic cellulose I peaks. Typical (1–10) peak at around 14.9° and (110) peak at 16.5° were overlapped to appear as a broad peak. The characteristic (200) peak appeared at ≈ 22.5°. These results imply that the DES treatment and mechanical defibrillation operations did not impact the cellulose

crystal structure. From the table, the crystallinity index (CrI) values clearly vary. The CrI values of all the DES-treated samples and LCNFs are higher than those of the raw materials, indicating that DES treatment removed the amorphous hemicellulose and lignin portions. Among the DES-treated samples, the MW-treated sample exhibited the highest CrI, and the 130°C sample exhibited the lowest value. Although the most hemicellulose and lignin were removed at 130°C, the crystallinity at this temperature was observed to be the lowest, which can be explained by the temperature effect. In a previous study, Shen et al. observed an increase in CrI from 54.8% to 60.2 and 68.3% when the temperature increased from 90°C to 100 and 110°C, respectively (Shen et al. 2019). However, a further increase to 120 and 130°C resulted in a decreased CrI of 62.3 and 58.1% respectively. This implies that the DES treatment temperature can improve the crystallinity to a certain extent but raising the temperature beyond this point is detrimental. The authors assumed that the high pretreatment temperature led to the cleavage of hydrogen bonds in lignocellulosic biomass and decreased the CrI of the substrates (Shen et al. 2019). In the current study, MW treatment might reach a high temperature, but high crystallinity is observed owing to the short duration, which might not cause hydrogen bond cleavage. By contrast, in conventional heating, with an increase in temperature from 110 to 130°C, the CrI decreased. The CrI values of the LCNFs are also shown in Table 1. In the case of MW, the CrI decreased after defibrillation. This observation is in accordance with the literature and can be ascribed to the disordering of the crystalline regions of the cellulose chain by the shear forces produced in the high-pressure homogenization process (Sánchez-Gutiérrez et al. 2020). However, in the case of heat treatment, the CrI increased after defibrillation, indicating that defibrillation was efficient. As evident from the morphological features, LCNF-110 and LCNF-130 were well defibrillated and during film preparation the crystalline regions might be well-aligned, resulting in improved CrI. In the case of LCNF-MW, this alignment might not occur and is still in disordered form owing to inefficient defibrillation. Additionally, Table 1 reveals that the average crystal sizes remained mostly unaltered after DES treatment and mechanical defibrillation, which is likely because cellulose is rarely hydrolyzed and destroyed (Liu et al. 2020).

Table 1
Crystallinity index (CrI%) and crystal widths of raw material, DES-treated samples, and LCNFs.

Sample		CrI (%)	Width (nm)
Raw material		51.5	2.2
MW	DES treatment	70.2	2.8
	Defibrillation	63.6	2.6
Conventional heating (110 ℃)	DES treatment	64.9	2.6
	Defibrillation	69.4	2.5
Conventional heating (130 ℃)	DES treatment	62.3	2.3
	Defibrillation	71.0	2.6

FT-IR analysis

FT-IR spectroscopy was used to study the chemical structure. The FTIR spectra of LCNFs produced by various DES pretreatments and the untreated wood sample are shown in Fig. 4b. In the case of the raw material, the peaks at 1594, 1508, 1262, and 808 cm^{-1} were attributed to lignin aromatic-ring vibrations, the guaiacyl ring vibration, C–O stretching of the acetyl group, and aromatic C–H stretching, respectively (Yang et al. 2007; Moubarik et al. 2013). The intensities of these peaks significantly decreased in the LCNFs, indicating the partial removal of lignin and hemicellulose. The peaks almost disappeared in LCNF-130, indicating its low amount of residual lignin. Although the lignin content of LCNF-110 is higher than that of LCNF-MW, the peaks were more prominent in LCNF-MW. Owing to the efficient defibrillation (as evidenced by SEM and TEM), the lignin nanoparticles might be uniformly distributed throughout the CNF matrix occupying the spaces between fibrils and become less exposed on the film surface. By contrast, in LCNF-MW, owing to inefficient defibrillation, most of the free lignin might be located on the surface of fibers and become available/exposed to the outer surface. The peak at 1736 cm^{-1} can be ascribed to the ester and protonated carboxylic acid in hemicellulose and lignin (Liu et al. 2019a). Interestingly, instead of decreasing, this peak increased after DES treatment, which can be attributed to the simultaneous occurrence of acid hydrolysis and esterification of cellulose upon CC/LA-DES treatment. During the treatment, the hydroxyl groups of cellulose undergo esterification with the carboxyl groups of lactic acid. This reaction was also observed previously (Liu et al. 2022b; Xie et al. 2023). In addition, the broad peak at $\approx$ 3400 cm^{-1} corresponding to the hydroxyl groups became more intense than that of the raw material. This suggests that the removal of lignin and hemicellulose exposes the hydroxyl groups of cellulose.

Strength properties

The effect of MW and conventional heat DES pretreatment on the mechanical properties of the LCNFs obtained by subsequent defibrillation was studied. The tensile strength, elongation at break (%), and elastic modulus of the LCNF films are presented in Table 2. Among the three LCNFs, LCNF-MW exhibited the worst mechanical properties (TS, EM, and elongation at break (%)), which can be ascribed to the inefficient defibrillation, as observed from the morphological characteristics. Nanosized cellulose fibers are known to exhibit better mechanical properties than macrosized fibers. LCNF-110 exhibited better tensile properties than LCNF-130. This result differs from those of previous reports, where samples treated at high temperature exhibited good mechanical properties (Xie et al. 2023), which was ascribed to their high lignin content. In well-defibrillated samples, to a certain extent, an increase in lignin content is known to enhance the mechanical properties by facilitating the stress transfer between CNFs (Farooq et al. 2019). However, an excessively high lignin content and/or inefficient defibrillation has a detrimental effect on the mechanical properties. In the case of LCNF-110, the uniform distribution of lignin throughout the CNF matrix was also supported by FTIR spectroscopy. Although LCNF-MW has a lignin content intermediate to the LCNF-110 and LCNF-130 samples, inefficient defibrillation is the main reason for its poor mechanical properties. Interestingly, the TS of the MW-treated sample is still comparable with TSs

reported in previous studies on LCNFs obtained by DES pretreatment. With the highest TS of 154.6 MPa, LCNF-110 finds great applicability as a packaging material and reinforcing agent.

Table 2
Strength properties of LCNFs

Sample	Tensile strength (MPa)	Elongation at break (%)	Young's modulus (GPa)
LCNF-MW	75.6 ± 1.4	7.5 ± 2.6	1.07 ± 0.4
LCNF-110	154.6 ± 5.0	9.9 ± 2.3	1.81 ± 0.2
LCNF-130	136.8 ± 1.2	8.0 ± 0.9	1.72 ± 0.2

Thermal stability

The thermal stability of the LCNF films was evaluated by TGA analysis, as shown in Fig. 5, and the corresponding thermal parameters, including T_{max} and residual weight (%) are presented in Table S1. As displayed in Fig. 5a, all three of the LCNFs exhibited three degradation stages: minor weight loss below 100°C can be ascribed to moisture loss; weight loss between 200 and 340°C might result from the degradation of hemicellulose and cellulose; and weight loss in the 340–600°C region was considered to be due to the slow pyrolysis of lignin (Xie et al. 2023). Owing to the low hemicellulose and lignin contents, LCNF-130 exhibited a high T_{onset} value but lowest T_{max} and residual content at 600°C. The low T_{onset} value of LCNF-MW and LCNF-110 can be ascribed to the presence of amorphous hemicellulose and lignin components. The T_{max} and residual contents of LCNF-110 and LCNF-MW were 305.4 and 309.6°C and 21.12 and 23.07%, respectively. These values are higher than that of LCNF-130 (297.9°C and 14.67%), implying that the residual lignin can increase thermal stability (Hong et al. 2020b). Interestingly, LCNF-MW with a lignin content less than that of LCNF-110 exhibited high thermal stability. This can be correlated with the FTIR and antioxidant activity results, which suggest that residual lignin present on the fiber surface of LCNF-MW protects it from thermal damage, and the reactivity of lignin in this form is lower (Peng et al. 2018). By contrast, in LCNF-110, lignin nanoparticles were distributed uniformly throughout the CNF matrix. As a whole, LCNF-MW exhibited good thermal stability.

Water contact angle

The hydrophilicity and hydrophobicity of the CNF films can be evaluated by measuring the water contact angles (WCAs). Materials with WCAs of less than 90° are considered hydrophilic, above 90° they are deemed hydrophobic, and above 150° they are classified as superhydrophobic (Simpson et al. 2015; Manoharan and Bhattacharya 2019). Pure CNF is known for its hydrophilicity. This might be an advantage for some applications like adsorbents, but for applications such as packaging and self-cleaning, hydrophobicity is required (Huang et al. 2021). Several strategies have been proposed to improve the hydrophobicity of CNF, and most of them involve harmful chemical modifications (Bayer

2020). Lignin present along with cellulose in biomass is a natural hydrophobic material, and retaining lignin is known to improve the hydrophobicity (Song et al. 2021). Here, the WCAs of the LCNFs obtained using MW and heat treatments were measured and are presented in Fig. 6. Although all three LCNFs have different lignin contents, there is no remarkable difference in their WCAs. Interestingly, all three samples exhibited a WCA greater than 87°, indicating their nearly hydrophobic nature, which can be advantageous for packing applications.

UV protection

Figure 7 depicts the transmittance of the LCNF films in the wavelength range of 190–900 nm. The detailed transmittance data of visible (T_{500nm}), UV A (T_{UVA}), and UV B (T_{UVB}) light is given in Table S2. The LCNF-130 film with 4.4% lignin exhibited high transmittance (54.07%) at T_{500nm}, and LCNF-110 with a high lignin content exhibited the lowest transmittance (36.89%). Interestingly, at a higher wavelength (700 nm), LCNF-110 exhibited the highest transmittance. The transmittance of LCNF-110 increased drastically with wavelength; above 550 nm it surpassed LCNF-MW, and above 650 nm it surpassed LCNF-130. At 800 nm, LCNF-110 exhibited the highest transmittance of 84.91%. Regardless of the high lignin content, this increased transmittance can be ascribed to its good defibrillation and uniform lignin dispersion, as evident from the tensile and FTIR results. All the samples exhibited excellent UVB protection (≈ 99%), and the UVA blocking varied depending on the lignin content. LCNF-110 with a high lignin content exhibited low UVA transmittance, whereas LCNF-130 with a low lignin content exhibited high transmittance. This UV-blocking nature can be ascribed to the phenolic structure of lignin (Sirviö et al. 2020). For a film to be applied for food packaging, good visible-light transparency and flexibility are required. Good transparency enables the consumer to view the packed food, and UV blocking ability is an added advantage because the food is protected from UV-light damage (Bian et al. 2021). As shown in Fig. 7b, all three LCNF films exhibited good transparency, as the pattern can be clearly seen. Furthermore, they tolerated bending, demonstrating their flexibility.

Antioxidant activity

Since free radicals are considered harmful to living organisms, exploring materials with radical scavenging ability (antioxidant activity) is of great interest (Dong et al. 2020). This antioxidant activity is especially desired for materials used to package food, cosmetics, and biomedicine to prevent them from spoilage (Espinosa et al. 2019). Lignin with a polyphenolic structure is capable of scavenging free radicals (Xiao et al. 2021), and LCNF with residual lignin is expected to exhibit antioxidant activity. Here, the antioxidant activity of the LCNF films was tested using an ABTS assay (Espinosa et al. 2019; Farooq et al. 2019). In a typical assay, ABTS was first converted to the positive radical ($ABTS^{\bullet+}$), which is blue in color and gives rise to a characteristic absorption peak at 730 nm. Upon incubation with LCNF, $ABTS^{\bullet+}$ absorbance decreases proportionally to LCNF's antioxidant potential. Figure 8a shows the absorption spectra of $ABTS^{\bullet+}$ after incubation with different CNF films, and the corresponding absorbance reduction is shown in Fig. 8b. PCNF without lignin exhibited low scavenging activity, whereas the LCNFs exhibited good antioxidant activity. Among the three LCNFs, LCNF-130 with the lowest lignin content exhibited the

lowest antioxidant activity. Interestingly, LCNF-MW with a lignin content lower than LCNF-110 exhibited the highest antioxidant activity. This can be ascribed to the inefficient defibrillation of LCNF-MW, where most of the free lignin might be located on the surface of fibers and become available/exposed on the outer surface. The high lignin peak intensities in the FTIR spectra and the higher thermal stability of LCNF-MW than LCNF-110 further support this assumption.

Conclusions

The successful production of LCNF from pine wood powder using microwave-assisted DES pretreatment and mechanical defibrillation was described. In addition, LCNFs were prepared via conventional heat treatment for comparison. MW treatment at 400 W for 110 s led to more efficient lignin and hemicellulose removal compared with conventional heat treatment at 110°C for 2 h. However, the morphological characteristics revealed inefficient defibrillation of the MW-treated sample, suggesting that MW treatment failed to induce the swelling effect that improves fiber susceptibility to defibrillation. Inefficient defibrillation was further confirmed by the poor mechanical properties. As indicated by the FT-IR spectra, residual lignin in LCNF-MW is highly exposed; as a result, LCNF-MW with a lignin content intermediate to that of LCNF-110 and LCNF-130 exhibited high thermal stability and antioxidant activity. LCNF-110 with high lignin content exhibited the best UV-blocking performance, and only a slight difference in WCA was observed. As a whole, this study compared LCNFs produced using DES pretreatment by conventional heating and MW heating.

Declarations

Acknowledgements

This research was supported by the Basic Science Research Program through the National Research Foundation of Korea (NRF), funded by the Ministry of Education (No. 2018R1A6A1A03025582).

Data availability

The authors confirm that the data supporting the findings of this study are available within the article and supporting information.

Funding

This research was supported by the Basic Science Research Program through the National Research Foundation of Korea (NRF), funded by the Ministry of Education (No. 2018R1A6A1A03025582).

Competing Interests

The authors have no relevant financial or non-financial interests to disclose.

References

1. A. Sluiter, B. Hames, R. Ruiz CS, Slui J, ter, D. Templeton and DC (2008) Determination of Structural Carbohydrates and Lignin in Biomass: Laboratory Analytical Procedure (LAP); Issue Date: April 2008; Revision Date: July 2011 (Version 07-08-2011) – 42618.pdf. Tech Rep NREL/ TP -510 -42618 1–15
2. Abbott AP, Capper G, Davies DL, et al (2003) Novel solvent properties of choline chloride/urea mixtures. Chem Commun 70–71. https://doi.org/10.1039/b210714g
3. Aguilar-Reynosa A, Romaní A, Ma. Rodríguez-Jasso R, et al (2017) Microwave heating processing as alternative of pretreatment in second-generation biorefinery: An overview. Energy Convers Manag 136:50–65. https://doi.org/10.1016/j.enconman.2017.01.004
4. Alvarez-Vasco C, Ma R, Quintero M, et al (2016) Unique low-molecular-weight lignin with high purity extracted from wood by deep eutectic solvents (DES): A source of lignin for valorization. Green Chem 18:5133–5141. https://doi.org/10.1039/c6gc01007e
5. Bayer IS (2020) Superhydrophobic Coatings from Ecofriendly Materials and Processes: A Review. Adv Mater Interfaces 7:1–25. https://doi.org/10.1002/admi.202000095
6. Bian H, Chen L, Dong M, et al (2021) Natural lignocellulosic nanofibril film with excellent ultraviolet blocking performance and robust environment resistance. Int J Biol Macromol 166:1578–1585. https://doi.org/10.1016/j.ijbiomac.2020.11.037
7. Chen Z, Bai X, Lusi A, Wan C (2018) High-Solid Lignocellulose Processing Enabled by Natural Deep Eutectic Solvent for Lignin Extraction and Industrially Relevant Production of Renewable Chemicals. ACS Sustain Chem Eng 6:12205–12216. https://doi.org/10.1021/acssuschemeng.8b02541
8. Dong H, Zheng L, Yu P, et al (2020) Characterization and Application of Lignin-Carbohydrate Complexes from Lignocellulosic Materials as Antioxidants for Scavenging in Vitro and in Vivo Reactive Oxygen Species. ACS Sustain Chem Eng 8:256–266. https://doi.org/10.1021/acssuschemeng.9b05290
9. Espinosa E, Bascón-Villegas I, Rosal A, et al (2019) PVA/(ligno)nanocellulose biocomposite films. Effect of residual lignin content on structural, mechanical, barrier and antioxidant properties. Int J Biol Macromol 141:197–206. https://doi.org/10.1016/j.ijbiomac.2019.08.262
10. Farooq M, Zou T, Riviere G, et al (2019) Strong, Ductile, and Waterproof Cellulose Nanofibril Composite Films with Colloidal Lignin Particles. Biomacromolecules 20:693–704. https://doi.org/10.1021/acs.biomac.8b01364
11. Francisco M, van den Bruinhorst A, Kroon MC (2012) New natural and renewable low transition temperature mixtures (LTTMs): screening as solvents for lignocellulosic biomass processing. Green Chem 14:2153. https://doi.org/10.1039/c2gc35660k
12. Gu L, Jiang B, Song J, et al (2019) Effect of lignin on performance of lignocellulose nanofibrils for durable superhydrophobic surface. Cellulose 26:933–944. https://doi.org/10.1007/s10570-018-2129-0
13. Herrera M, Thitiwutthisakul K, Yang X, et al (2018) Preparation and evaluation of high-lignin content cellulose nanofibrils from eucalyptus pulp. Cellulose 25:3121–3133. https://doi.org/10.1007/s10570-018-1764-9

14. Hong S, Shen XJ, Xue Z, et al (2020a) Structure-function relationships of deep eutectic solvents for lignin extraction and chemical transformation. Green Chem. 22:7219–7232
15. Hong S, Song Y, Yuan Y, et al (2020b) Production and characterization of lignin containing nanocellulose from luffa through an acidic deep eutectic solvent treatment and systematic fractionation. Ind Crops Prod 143:111913. https://doi.org/10.1016/j.indcrop.2019.111913
16. Huang J, Li M, Lu Y, et al (2021) A facile preparation of superhydrophobic L-CNC-coated meshes for oil-water separation. RSC Adv 11:13992–13999. https://doi.org/10.1039/d1ra02291a
17. Impoolsup T, Chiewchan N, Devahastin S (2020) On the use of microwave pretreatment to assist zero-waste chemical-free production process of nanofibrillated cellulose from lime residue. Carbohydr Polym 230:115630. https://doi.org/10.1016/j.carbpol.2019.115630
18. Ji Q, Yu X, Yagoub AEGA, et al (2021) Efficient cleavage of strong hydrogen bonds in sugarcane bagasse by ternary acidic deep eutectic solvent and ultrasonication to facile fabrication of cellulose nanofibers. Cellulose 28:6159–6182. https://doi.org/10.1007/s10570-021-03876-w
19. Kumar AK, Parikh BS, Pravakar M (2016) Natural deep eutectic solvent mediated pretreatment of rice straw: bioanalytical characterization of lignin extract and enzymatic hydrolysis of pretreated biomass residue. Environ Sci Pollut Res 23:9265–9275. https://doi.org/10.1007/s11356-015-4780-4
20. Kwon GJ, Bandi R, Yang BS, et al (2021) Choline chloride based deep eutectic solvents for the lignocellulose nanofibril production from Mongolian oak (Quercus mongolica). Cellulose 28:9169–9185. https://doi.org/10.1007/s10570-021-04102-3
21. Kwon GJ, Yang BS, Park CW, et al (2020) Treatment effects of choline chloride-based deep eutectic solvent on the chemical composition of red pine (Pinus densiflora). BioResources 15:6457–6470. https://doi.org/10.15376/biores.8.3.6457-6470
22. Liu C, Li MC, Chen W, et al (2020) Production of lignin-containing cellulose nanofibers using deep eutectic solvents for UV-absorbing polymer reinforcement. Carbohydr Polym 246:116548. https://doi.org/10.1016/j.carbpol.2020.116548
23. Liu C, Li Z, Li MC, et al (2022a) Lignin-containing cellulose nanofibers made with microwave-aid green solvent treatment for magnetic fluid stabilization. Carbohydr Polym 291:119573. https://doi.org/10.1016/j.carbpol.2022.119573
24. Liu C, Zhou G, Li Z, et al (2022b) Lignin-containing cellulose nanomaterials produced by microwave-assisted deep eutectic solvent treatment as rheology modifiers for fracturing fluids. Ind Crops Prod 187:115402. https://doi.org/10.1016/j.indcrop.2022.115402
25. Liu Q, Yuan T, Fu Q, et al (2019a) Choline chloride-lactic acid deep eutectic solvent for delignification and nanocellulose production of moso bamboo. Cellulose 26:9447–9462. https://doi.org/10.1007/s10570-019-02726-0
26. Liu Y, Chen W, Xia Q, et al (2017a) Efficient Cleavage of Lignin–Carbohydrate Complexes and Ultrafast Extraction of Lignin Oligomers from Wood Biomass by Microwave-Assisted Treatment with Deep Eutectic Solvent. ChemSusChem 10:1692–1700. https://doi.org/10.1002/cssc.201601795

27. Liu Y, Guo B, Xia Q, et al (2017b) Efficient Cleavage of Strong Hydrogen Bonds in Cotton by Deep Eutectic Solvents and Facile Fabrication of Cellulose Nanocrystals in High Yields. ACS Sustain Chem Eng 5:7623–7631. https://doi.org/10.1021/acssuschemeng.7b00954
28. Liu Y, Nie Y, Lu X, et al (2019b) Cascade utilization of lignocellulosic biomass to high-value products. Green Chem 21:3499–3535. https://doi.org/10.1039/C9GC00473D
29. Lynam JG, Kumar N, Wong MJ (2017) Deep eutectic solvents' ability to solubilize lignin, cellulose, and hemicellulose; thermal stability; and density. Bioresour Technol 238:684–689. https://doi.org/10.1016/j.biortech.2017.04.079
30. Manoharan K, Bhattacharya S (2019) Superhydrophobic surfaces review: Functional application, fabrication techniques and limitations. J Micromanufacturing 2:59–78. https://doi.org/10.1177/2516598419836345
31. Moubarik A, Grimi N, Boussetta N (2013) Structural and thermal characterization of Moroccan sugar cane bagasse cellulose fibers and their applications as a reinforcing agent in low density polyethylene. Compos Part B Eng 52:233–238. https://doi.org/10.1016/j.compositesb.2013.04.040
32. Nair SS, Yan N (2015a) Effect of high residual lignin on the thermal stability of nanofibrils and its enhanced mechanical performance in aqueous environments. Cellulose 22:3137–3150. https://doi.org/10.1007/s10570-015-0737-5
33. Nair SS, Yan N (2015b) Bark derived submicron-sized and nano-sized cellulose fibers: From industrial waste to high performance materials. Carbohydr Polym 134:258–266. https://doi.org/10.1016/j.carbpol.2015.07.080
34. Peng Y, Nair SS, Chen H, et al (2018) Effects of Lignin Content on Mechanical and Thermal Properties of Polypropylene Composites Reinforced with Micro Particles of Spray Dried Cellulose Nanofibrils. ACS Sustain Chem Eng 6:11078–11086. https://doi.org/10.1021/acssuschemeng.8b02544
35. Rojo E, Peresin MS, Sampson WW, et al (2015) Comprehensive elucidation of the effect of residual lignin on the physical, barrier, mechanical and surface properties of nanocellulose films. Green Chem 17:1853–1866. https://doi.org/10.1039/c4gc02398f
36. Sánchez-Gutiérrez M, Espinosa E, Bascón-Villegas I, et al (2020) Production of Cellulose Nanofibers from Olive Tree Harvest—A Residue with Wide Applications. Agronomy 10:696. https://doi.org/10.3390/agronomy10050696
37. Satlewal A, Agrawal R, Bhagia S, et al (2018) Natural deep eutectic solvents for lignocellulosic biomass pretreatment: Recent developments, challenges and novel opportunities. Biotechnol Adv 36:2032–2050. https://doi.org/10.1016/j.biotechadv.2018.08.009
38. Shen XJ, Wen JL, Mei QQ, et al (2019) Facile fractionation of lignocelluloses by biomass-derived deep eutectic solvent (DES) pretreatment for cellulose enzymatic hydrolysis and lignin valorization. Green Chem 21:275–283. https://doi.org/10.1039/c8gc03064b
39. Simpson JT, Hunter SR, Aytug T (2015) Superhydrophobic materials and coatings: A review. Reports Prog Phys 78:. https://doi.org/10.1088/0034-4885/78/8/086501

40. Sirviö JA, Ismail MY, Zhang K, et al (2020) Transparent lignin-containing wood nanofiber films with UV-blocking, oxygen barrier, and anti-microbial properties. J Mater Chem A 8:7935–7946. https://doi.org/10.1039/c9ta13182e
41. Sirviö JA, Visanko M, Liimatainen H (2015) Deep eutectic solvent system based on choline chloride-urea as a pre-treatment for nanofibrillation of wood cellulose. Green Chem 17:3401–3406. https://doi.org/10.1039/c5gc00398a
42. Smith EL, Abbott AP, Ryder KS (2014) Deep Eutectic Solvents (DESs) and Their Applications. Chem. Rev. 114:11060–11082
43. Song Y, Xu Y, Li D, et al (2021) Sustainable and Superhydrophobic Lignocellulose-Based Transparent Films with Efficient Light Management and Self-Cleaning. ACS Appl Mater Interfaces 13:49340–49347. https://doi.org/10.1021/acsami.1c14948
44. Trovagunta R, Zou T, Osterberg M, et al (2020) Design strategies, properties and application of cellulose nanomaterials-enhanced products with residual, technical or nanoscale lignin – A review. Carbohydr Polym Submitted: https://doi.org/10.1016/j.carbpol.2020.117480
45. Wang H, Li J, Zeng X, et al (2020) Extraction of cellulose nanocrystals using a recyclable deep eutectic solvent. Cellulose 27:1301–1314. https://doi.org/10.1007/s10570-019-02867-2
46. Wang Q, Du H, Zhang F, et al (2018) Flexible cellulose nanopaper with high wet tensile strength, high toughness and tunable ultraviolet blocking ability fabricated from tobacco stalk: Via a sustainable method. J Mater Chem A 6:13021–13030. https://doi.org/10.1039/c8ta01986j
47. Wen Y, Yuan Z, Liu X, et al (2019) Preparation and Characterization of Lignin-Containing Cellulose Nanofibril from Poplar High-Yield Pulp via TEMPO-Mediated Oxidation and Homogenization. ACS Sustain Chem Eng 7:6131–6139. https://doi.org/10.1021/acssuschemeng.8b06355
48. Xiao L, Liu W, Huang J, et al (2021) Study on the Antioxidant Activity of Lignin and Its Application Performance in SBS Elastomer. Ind Eng Chem Res 60:790–797. https://doi.org/10.1021/acs.iecr.0c04699
49. Xie J, Xu J, Zhang Z, et al (2023) New ternary deep eutectic solvents with cycle performance for efficient pretreated radiata pine forming to lignin containing cellulose nanofibrils. Chem Eng J 451:138591. https://doi.org/10.1016/j.cej.2022.138591
50. Yang H, Yan R, Chen H, et al (2007) Characteristics of hemicellulose, cellulose and lignin pyrolysis. Fuel 86:1781–1788. https://doi.org/10.1016/j.fuel.2006.12.013
51. Zdanowicz M, Wilpiszewska K, Spychaj T (2018) Deep eutectic solvents for polysaccharides processing. A review. Carbohydr. Polym. 200:361–380

Figures

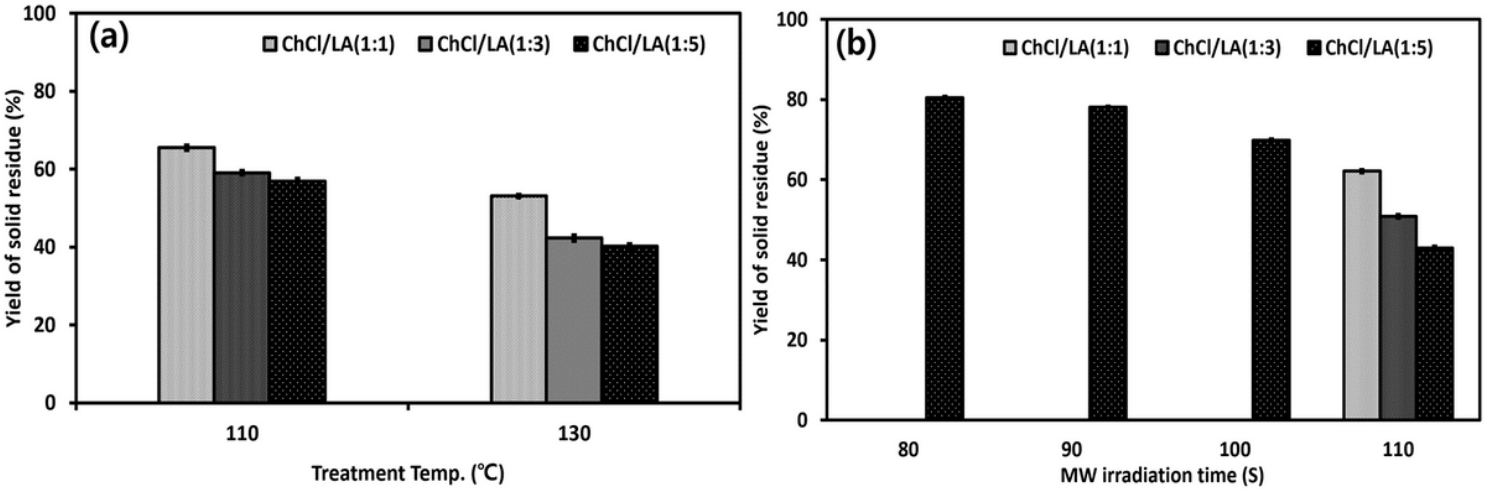

Figure 1

Yield of solid residue obtained after DES treatment under different conditions: **a** conventional heating and **b** microwave heating

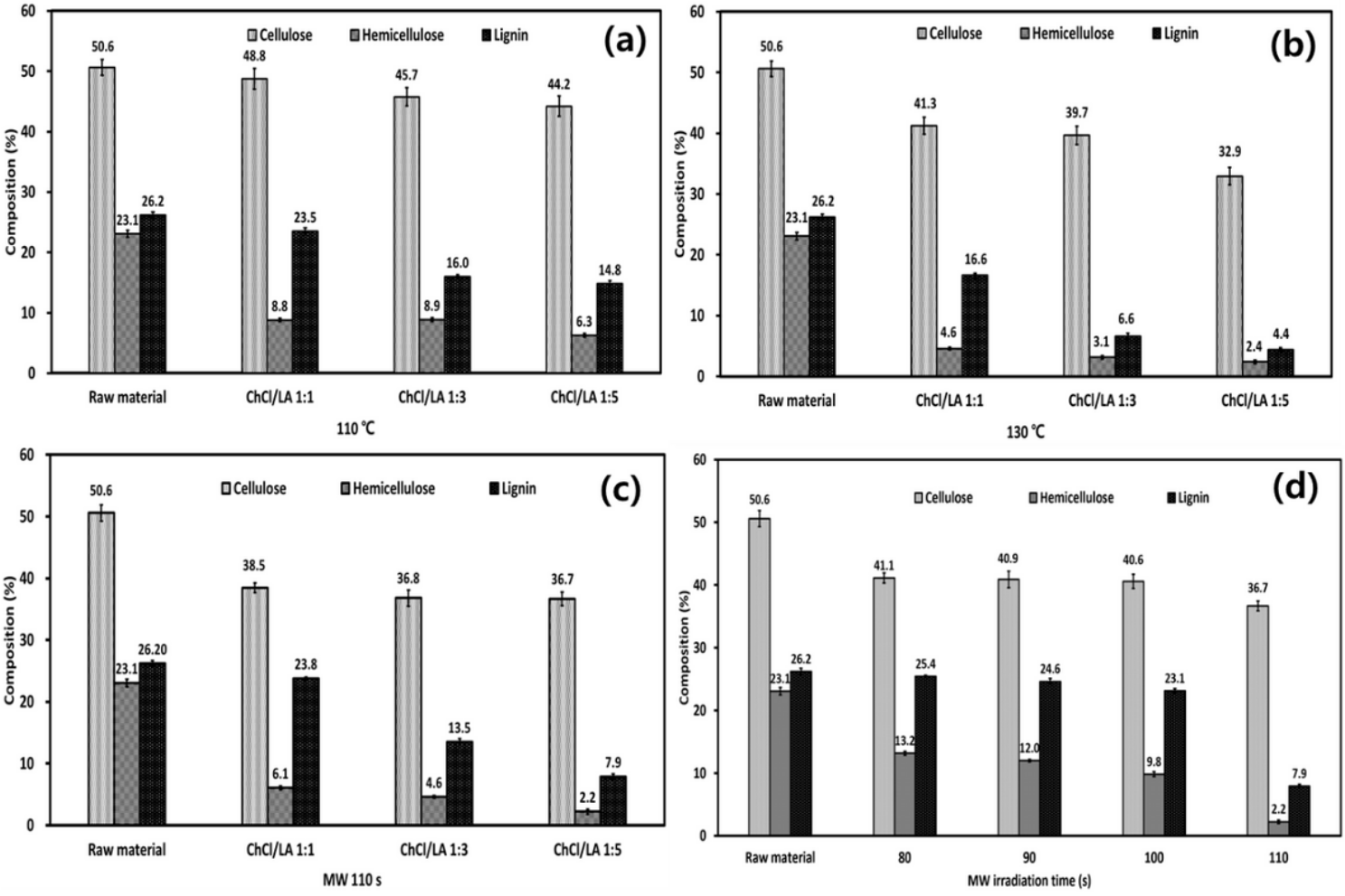

Figure 2

Chemical composition of DES-treated residues obtained under various conditions: mole ratio variation at **a** 110 °C, **b** 130 °C, and **c** MW heating. **d** MW irradiation time variation

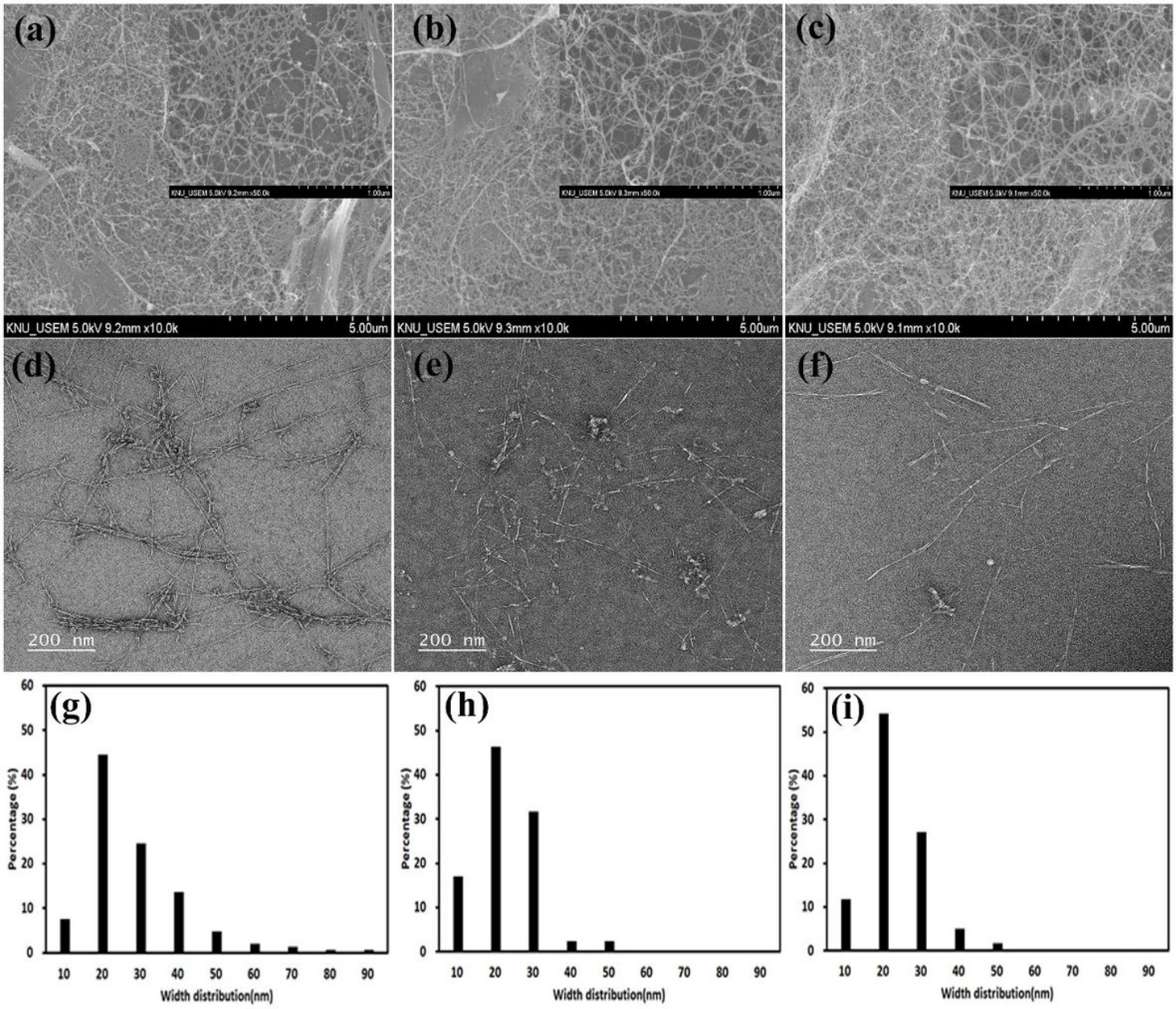

Figure 3

SEM images (**a–c**), TEM images (**d–f**), and corresponding diameter distribution histograms (**g–i**) of LCNF-MW (**a,d,g**), LCNF-110 (**b,e,h**), and LCNF-130 (**c,f,i**)

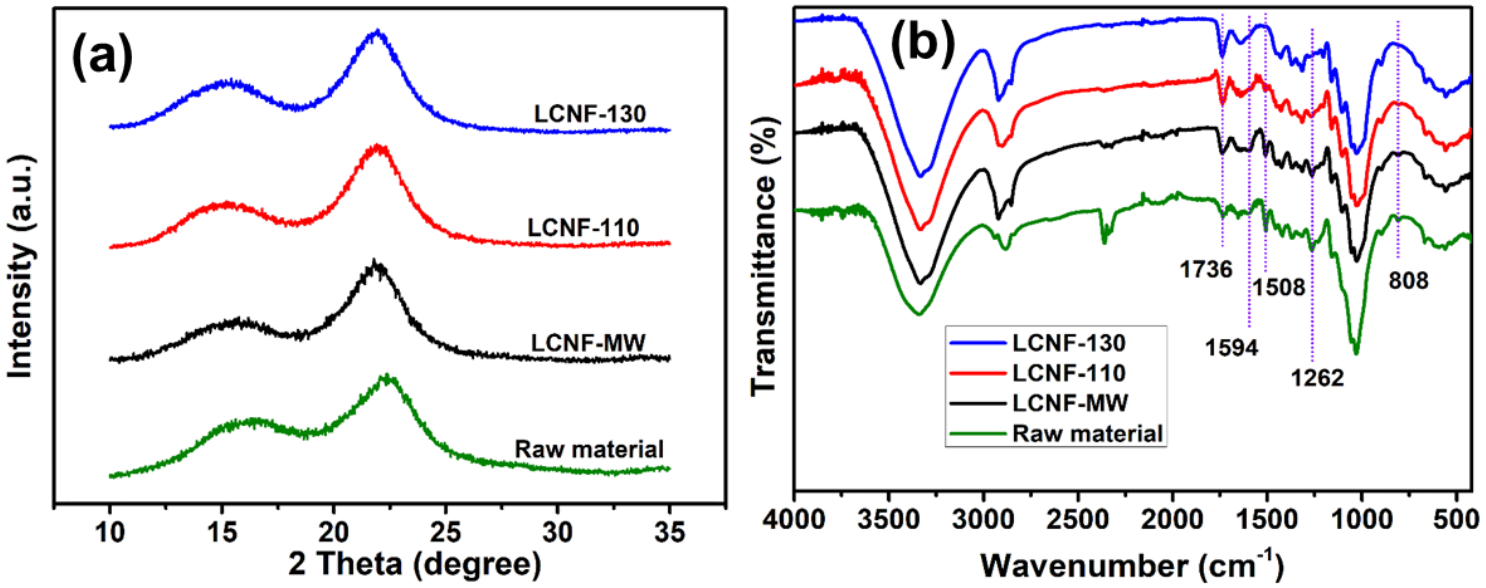

Figure 4

(**a**) XRD patterns and **b** FT-IR spectra of raw material and LCNFs

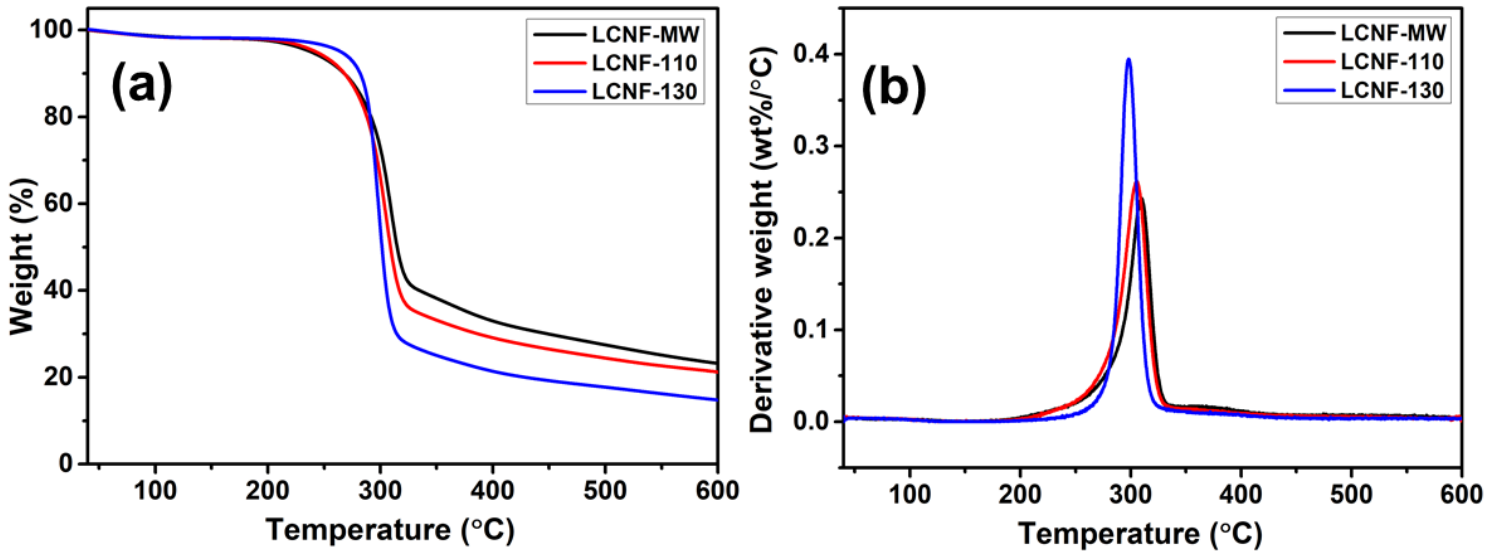

Figure 5

a TGA and **b** DTG curves of LCNFs

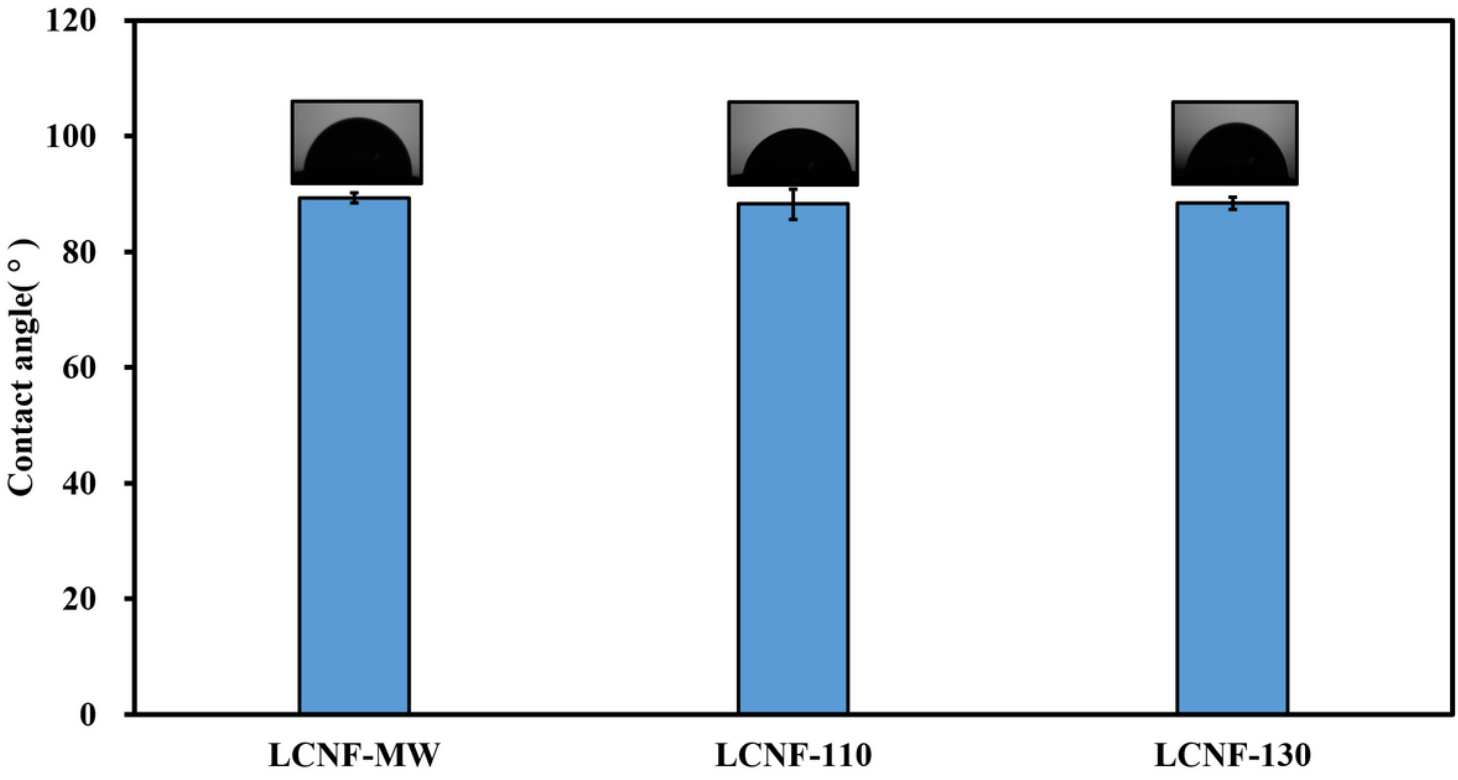

Figure 6

Water contact angles of LCNF-MW, LCNF-110. and LCNF-130

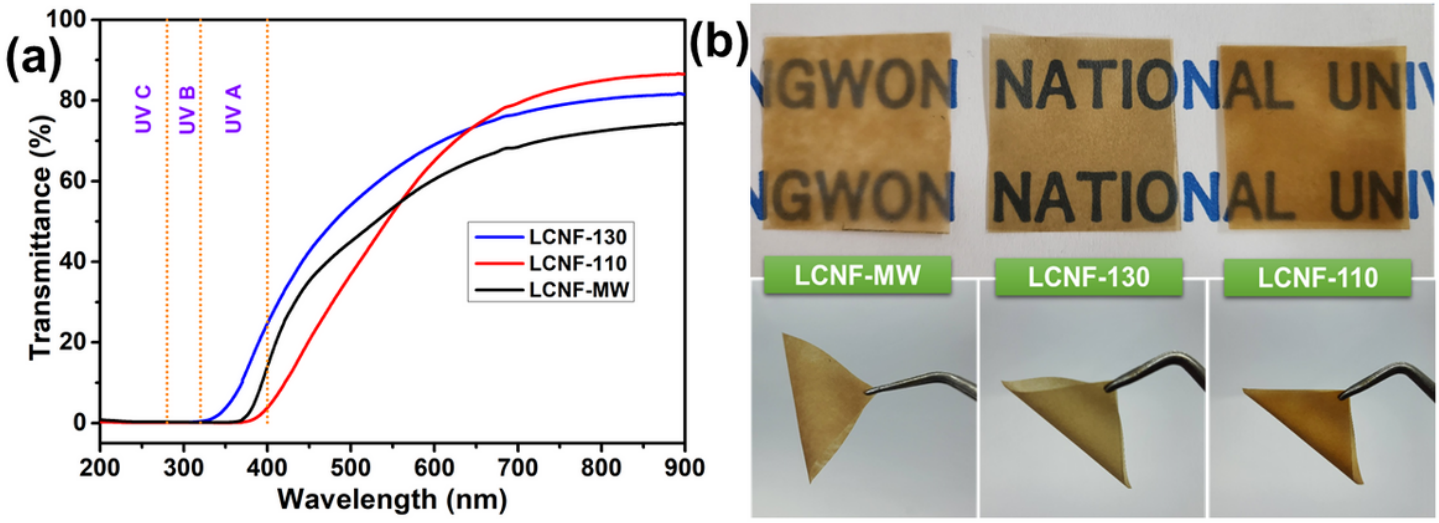

Figure 7

a UV–vis transmission spectra and **b** digital photographs of the LCNF films

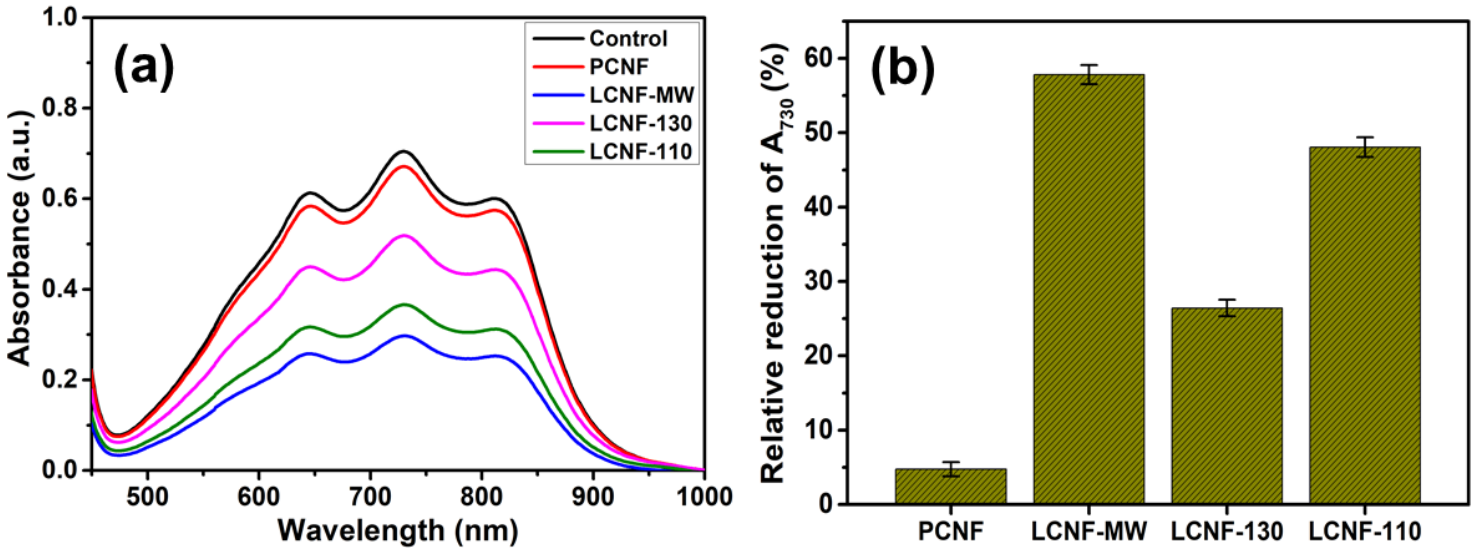

Figure 8

Antioxidant activity: **a** absorption spectra of ABTS in the presence of different CNF films and **b** corresponding relative reduction in ABTS absorption

Supplementary Files

This is a list of supplementary files associated with this preprint. Click to download.

- Supportinginformation.docx